Applied Physics Letters

Study on near-field acoustic levitation characteristics in a pressurized environment

Cite as: Appl. Phys. Lett. **120**, 034103 (2022); https://doi.org/10.1063/5.0075193
Submitted: 14 October 2021 • Accepted: 04 January 2022 • Published Online: 18 January 2022

Ronghe Li, Yifei Li, Hande Sang, et al.

AIP Publishing

Applied Physics Letters ARTICLE scitation.org/journal/apl

Study on near-field acoustic levitation characteristics in a pressurized environment

Cite as: Appl. Phys. Lett. **120**, 034103 (2022); doi: 10.1063/5.0075193
Submitted: 14 October 2021 · Accepted: 4 January 2022 ·
Published Online: 18 January 2022

Ronghe Li,[1,2] Yifei Li,[1] Hande Sang,[1,2] Yuanyuan Liu,[3] Shuang Chen,[2] and Su Zhao[1,a)]

AFFILIATIONS

[1]Ningbo Institute of Materials Technology and Engineering, Chinese Academy of Sciences, Ningbo 315200, China
[2]School of Mechanical and Electrical Engineering, Jiangxi University of Science and Technology, Ganzhou 341000, China
[3]Chair of Vibroacoustics of Vehicles and Machines, Technical University of Munich, Garching 85748, Germany

[a)]Author to whom correspondence should be addressed: zhaosu@nimte.ac.cn

ABSTRACT

The influence of the ambient pressure on the load capacity of near-field acoustic levitation is studied. Theoretical models based on the acoustic radiation pressure and hydrodynamic lubrication theory are built, taking into account the changes of the ambient pressure. Both simulation and measured results show that the levitation force is positively proportional to the ambient pressure. The levitation force increased by 4–5 times at an ambient pressure of 0.5 MPa. A maximum load capacity of 0.309 MPa is obtained.

The near-field acoustic levitation (NFAL) system is composed of two plates: a radiator and a reflector [see Fig. 1(a)]. The gap between the two plates is usually in micrometer range. When the radiator vibrates at high frequency, the gas within the gap has not enough time to flow in or out. Therefore, the gas film is expanded and compressed rapidly, and the pressure in the gap changes periodically. However, due to the nonlinearity of the gas, pressure oscillation caused by a harmonic motion is non-harmonic. The effect is shown in Fig. 1(b) qualitatively,[1] where h_0 is the initial levitation distance, a_0 is the vibration amplitude, p_{max} is the maximum pressure, p_{min} is the minimum pressure, and t is the time. The time averaged pressure $\bar{p}$ is higher than the ambient pressure p_b. Therefore, a repelling levitation force is generated in the gap.

Since the NFAL phenomenon was discovered by Salbu[2] in 1964 through the study of squeeze film bearings, significant progress has been made in theoretical studies and engineering applications.[3–6] A rotational bearing excited by three piezoelectric transducers was proposed by Zhao *et al.*[7] in 2009. Based on this study, Liu *et al.*[8] studied the static and dynamic characteristics of the squeeze film bearing in 2021. A NFAL bearing with a similar structure was proposed by Li *et al.*[9] The bearing with a self-aligning function has radial and axial load-carrying capacity. The maximum radial load-carrying capacity per unit area of the bearing is 0.038 MPa, and the maximum axial load-carrying capacity is 0.004 MPa. A self-running and self-floating actuator was designed by Chen *et al.*[10] in 2016. Experimental results show that the load capacity of the actuator can reach 0.8 N. Andrade *et al.*[11] discovered the inverted near-field acoustic levitation phenomenon in 2020 and applied this phenomenon to a contactless pick-and-place device. An object with a weight of 9 mg was suspended. A squeeze film air bearing with a flexure pivot tilting pad was proposed by Shi *et al.*[12] in 2017, and this structure is suitable for high speed and light load conditions. Two different types of system stiffness models were defined by Wang and Guo[13] to study the characteristics of the NFAL bearing in 2021.

NFAL is a promising technique for contactless support and handling. However, the application of this technique is often limited by its relatively low load capacity. Comparing with aerostatic and electromagnetic bearings, the load capacity of the squeeze film bearing is much lower. The highest reported load capacity is 0.062 MPa by Zhao *et al.*[7] According to previous studies, the levitation force can be improved by increasing the amplitude or reducing the levitation distance. However, due to limited material strength, the vibration amplitude cannot be infinitely increased. The levitation distance is also limited by the machining accuracy of the matching surfaces. From reported theoretical models, it can be derived that the higher ambient pressure could lead to a higher levitation force. However, no related research has been found in previously reported works. This paper will focus on the theoretical and experimental investigation of the relationship between the ambient pressure and the levitation force.

Theoretical models describing the NFAL system are mostly developed based on the theory of linear acoustics and hydrodynamics.[2,4–6,14,15] The most classical models are adopted to describe the relationship between the levitation force and the ambient pressure in this study.

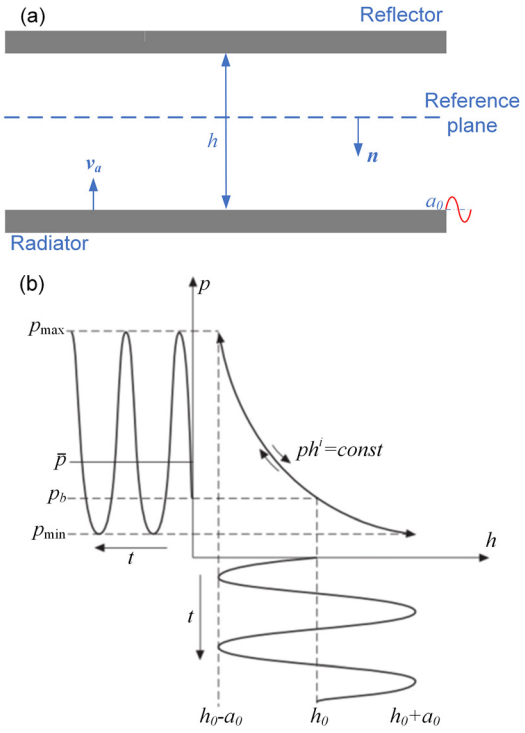

FIG. 1. (a) Schematic diagram of the near-field acoustic levitation system. (b) The non-harmonic pressure oscillation caused by a harmonic motion.[1]

The average acoustic radiation pressure per unit time $\bar{p}$ was derived by Lee and Wang[16,17] as

$$\bar{p} = \langle p_a - p_b \rangle = \left(\frac{\gamma - 1}{2} + \cos 2kz \right) \frac{a_0^2 c_a^2 \rho_a}{4h_0^2}, \tag{1}$$

where p_a is the acoustic radiation pressure between the two surfaces, p_b is the ambient pressure, γ is the specific heat ratio (γ= 1.4 for air), a_0 is the vibration amplitude, ρ_a is the air density, c_a is the speed of sound in air, k is the wave number, z is the acoustic transmission distance, and h_0 is the initial levitation distance between the radiator and the reflector. $\cos 2kz$ can be approximated as one because of the micrometer level of the sound transmission distance. Thus, Eq. (1) can be expressed as[16,17]

$$\bar{p} = \frac{\gamma + 1}{8} \frac{a_0^2 c_a^2 \rho_a}{h_0^2}. \tag{2}$$

The speed of sound can be expressed as

$$c_a = \sqrt{\frac{\gamma p_b}{\rho_a}}. \tag{3}$$

Substituting Eq. (3) into Eq. (2), the acoustic radiation pressure per unit time is obtained as

$$\bar{p} = \frac{\gamma(\gamma + 1)}{8} \frac{a_0^2 p_b}{h_0^2}. \tag{4}$$

The levitation force can be obtained by integrating the overlapping area of the radiated sound pressure on the radiator and reflector, which is stated as

$$F = \int \bar{p} dS. \tag{5}$$

Equation (4) shows that the levitation force is directly proportional to the ambient pressure.

The Reynolds equation describing the pressure distribution between two relatively moving surfaces based on the one-dimensional axisymmetric Navier–Stokes equation is expressed by[18]

$$\frac{\partial}{\partial x} \left(\frac{\rho_a h^3}{12\eta} \frac{\partial p}{\partial x} \right) = \frac{\partial (\rho_a h)}{\partial t}, \tag{6}$$

where x is the Cartesian coordinate in the direction of the gap, t is the time, η is the dynamic viscosity, and p is the pressure within the gap. The dynamic distance between the two surfaces can be expressed as

$$h(t) = h_0 + a_0 \sin \omega t. \tag{7}$$

In order to reduce the number of parameters, discuss the results, and improve the stability of the model, all variables in Eq. (6) need to be dimensionless. The dimensionless parameters of this model are defined as

$$\sigma = \frac{12\omega\eta L^2}{p_b h_0^2}, \quad P = \frac{p}{p_0}, \quad H = \frac{h}{h_0}, \quad X = \frac{x}{L}, \quad T = \omega t, \tag{8}$$

where σ is the squeeze number, which describes the intensity of the squeezing action of the two surfaces, p_0 is the characteristic pressure,

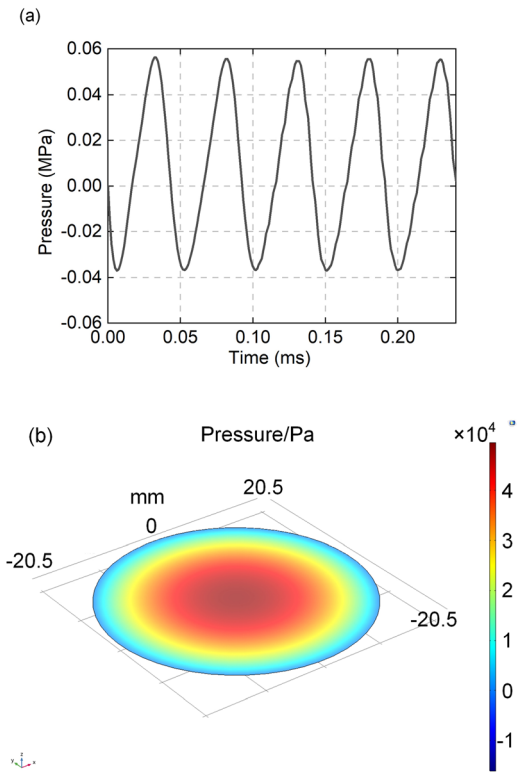

FIG. 2. (a) FEM simulation result of the instantaneous pressure distribution of the gas film. (b) Instantaneous pressure in the gap.

h_0 is the characteristic length in the z-direction (initial levitation distance), L is the characteristic length of the gas film, and ω is the angular speed. Substituting Eq. (8) into Eq. (6), we obtain[18]

$$\frac{\partial}{\partial X}\left(PH^3\frac{\partial P}{\partial X}\right)=\sigma\frac{\partial(PH)}{\partial T}. \tag{9}$$

The initial and boundary conditions are as follows:

$$\begin{cases}\text{Initial condition}: P(X,T=0)=P_1,\\ \text{Boundary condition 1}: P\left(X=\frac{1}{2},T\right)=P_1,\\ \text{Boundary condition 2}: \frac{\partial P(X=0,T)}{\partial x}=0,\end{cases} \tag{10}$$

where P_1 is the dimensionless ambient pressure. Equations (9) and (10) are solved using the finite difference method.

The finite element method (FEM) is also applied to calculate the NFAL force using the COMSOL Multiphysics software. The model analyzes the influence of the periodic movement of the radiator surface on the fluid flow, including the gas pressure and the resulting levitation force. The levitation force is generated by the extrusion and compression of a gas film between two surfaces. In this model, the "thin-film flow, edge interface" module is adopted to model the pressure distribution of the gas film. The boundary condition of the model is that the pressure at the edge of the gas film equals to the ambient pressure, and the gradient of the pressure at the center of the film along the radius direction is zero. The model is one-dimensional axisymmetric since the film pressure only varies radially. The mesh is set as "extra fine" through the physics-controlled mesh. The only material parameter related to the modified Reynolds equation is the dynamic viscosity of air, which is 1.8448×10^{-5} Pa·s at 25 °C. For high frequency and large amplitude vibration, the levitation force is nonlinear with respect to

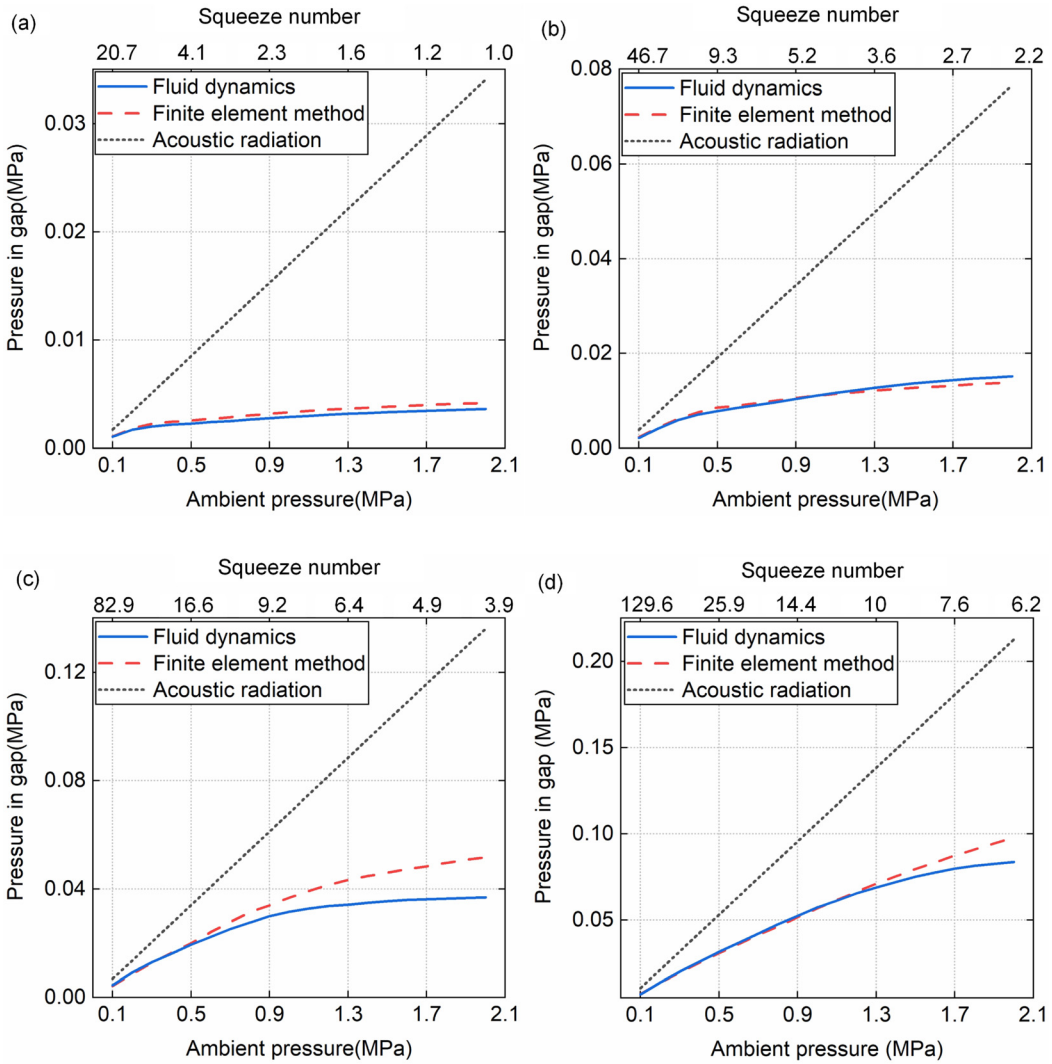

FIG. 3. Comparison of average pressure obtained from different models. (a) $h=150$ μm. (b) $h=100$ μm. (c) $h=75$ μm. (d) $h=60$ μm.

the harmonic motion of the radiator surface. Therefore, transient analysis of the model is carried out.

The configuration of film flow in the gap is shown in Fig. 1(a). The reference plane with the normal direction $\boldsymbol{n}$ is between the radiator and the reflector. The vector $\boldsymbol{n}$ points into the radiator surface. The initial velocity of the radiator surface is expressed as $\boldsymbol{v}_a$. The transient model of the modified Reynolds equation is[18]

$$\frac{\partial}{\partial t}(p_t h) + \nabla_t \cdot (h p_t \boldsymbol{v}_0) - p_t(\boldsymbol{v}_a \cdot \nabla_t a_0) = 0, \tag{11}$$

where ∇_t is the gradient operator, the in-plane vector $\boldsymbol{v}_0$ is the average film velocity perpendicular to the radiator surface, $\hat{p}$ is the transient pressure generated by the gas film flow, p_t is the total pressure ($p_t = \hat{p} + p_b$), and $\mathbf{I}$ is the identity matrix. The average film velocity can be calculated as[18]

$$\boldsymbol{v}_0 = \frac{1}{2}(\mathbf{I} - \boldsymbol{n}\boldsymbol{n}^T)\boldsymbol{v}_a - \frac{h^2}{12\eta}\nabla_t \hat{p}. \tag{12}$$

For larger vibration amplitudes, the response in terms of pressure is nonlinear with respect to the applied harmonic motion of the radiator. Therefore, transient analysis is carried out to solve the modified Reynolds equation. Figure 2(a) shows the calculated instantaneous pressure in the gap (averaged over the length) caused by the vibration of the transducer surface. The vibration amplitude is set as 30 μm with a frequency of 20.5 kHz. The initial gap distance is set as 75 μm. It can be seen that the pressure in the gap changes periodically with the simple harmonic vibration of the radiator. The absolute value of the negative pressure is 0.037 MPa, which is lower than the positive pressure (0.056 MPa). Figure 2(b) shows the pressure distribution over the gap at the time point when the radiator surface moves to the nearest position to the reflector. It can be observed that the pressure is equal to the ambient pressure at the edge of the gap and gradually increases to the maximum while moving toward the center of the gap.

The time averaged pressure in the gap at different ambient pressures is calculated using the three presented models and plotted together in Fig. 3. The levitation distances are set as 150, 100, 75, and 60 μm when the vibration amplitude is set as 30 μm. The levitation pressure obtained from all three models is positively correlated with the ambient pressure. The results show that it is an effective method to improve the load capacity of NFAL by increasing the ambient pressure. The three models show obvious disagreements at different levitation parameters. The model based on the acoustic radiation pressure theory is heavily simplified, which shows a simple linear relation at all different levitation parameters. On the other hand, the two models based on the fluid dynamics theory give better insight of the levitation mechanism because they consider gas viscosity and boundary conditions of the levitation gap. When the levitation distances are set relatively at 150 and 100 μm, the two models based on fluid dynamics theory give similar results [see Figs. 3(a) and 3(b)]. For small gap [Figs. 3(c) and 3(d)], the results from two fluid dynamics models show increasing difference at the higher ambient pressure. The difference could be caused by the different solving methods used.

An experimental setup is constructed to measure the levitation force in a pressurized environment, as shown in Fig. 4. A Langevin type piezoelectric transducer (Model: Resotek R20-6) with a central frequency of 20.5 kHz is employed to drive a whole wavelength booster with a radiating surface of 41 mm in diameter to provide piston-like vibration. The system is driven by a PWM controlled full-bridge switching ultrasonic generator made by Resotek Co. Ltd. (Model: ResoGen-3000). A plate is mounted on a force sensor (Model: Kistler 9323AAA; Linearity: 0.11%) through a ball socket bearing (Model: Hephaist SRJ024C). The ball socket bearing has high precision, low rotation resistance, and zero clearance. If the reflector tilts, the lower side of the reflector will bear higher levitation force resulted from the smaller gap distance. Therefore, the reflector is kept parallel to the radiator by the distributed levitation force during the levitation process. The sound radiator, reflector, ball socket bearing, and force sensor are sealed in a transparent pressure vessel. The lower end of the vessel is sealed at the flange of the booster. The force sensor is connected with a linear module (Model: IKO TZ200X-4; Resolution: 1.25 μm/pulse) through a shaft, which goes through the upper end of the pressure vessel with a sliding seal. The force sensor is matched with a charge amplifier (Model: Kistler 5015) to record the forces.

The amplitude of the radiator is measured by a single-point laser-Doppler-vibrometer (Model: LV-S01 from Sunny Optical Intelligent Technology Co, Ltd., accuracy: 0.001 μm). The bandpass filter was set to 1–50 kHz. A mapping between the output power level of the ultrasonic generator and the vibration amplitudes is carried out. During the experiment, desired amplitude can be obtained by setting the output power to the corresponding power level. The measured

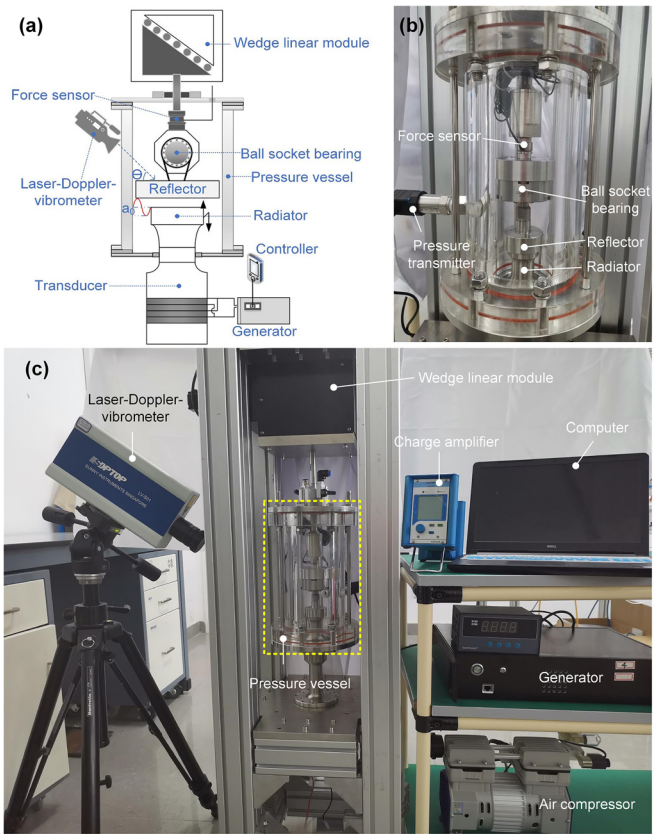

FIG. 4. Experimental setup. (a) Schematic diagram. (b) Partially enlarged view. (c) Overall view.

vibration waveform is pure with a single peak in the frequency domain (20.5 kHz), with no obvious higher or lower harmonics observed. The vibration amplitude of the radiator is kept at 30 μm (peak) for all measurements. The pressure in the vessel is regulated to the desired values by an external air pump and a pressure gauge. Due to the limitation of the withstanding capacity of the pressure vessels, the pressure is increased to a maximum of 0.5 MPa with an interval of 0.05 MPa.

Levitation forces at different pressures are measured at four different levitation distances of 150, 100, 75, and 60 μm. Before each measurement, the pressure in the vessel is adjusted to set value at first. Second, the two levitation surfaces are brought into contact. Then, the gap distance is increased to the set value by driving the linear module. This procedure eliminates the part movement caused by the change of the internal pressure. When the desired gap distance is reached, the ultrasonic generator is turned on to create levitation force, which is measured by the force sensor. Temperature rise in the gap is observed during the levitation process. With a gap distance of 60 μm and above, the temperature raised about 5 °C after 30 s. To avoid the influence of temperature rise on the levitation forces, the force measurements were completed within 5 s after the generator is turned on.

The displacement of the reflector is also measured by the laser-Doppler-vibrometer during the experiment to verify the true gap distance. The displace measurement is done at 45° angle, which is calculated back to the vertical displacement [see Fig. 4(a)]. Each measurement is repeated three times and then averaged to minimize error introduced by operation.

The measured levitation forces at different ambient pressure and levitation distances are plotted in Fig. 5 together with the calculated results. The resulting squeeze number of different pressures is shown as well. It can be observed that the levitation forces increase significantly with higher ambient pressure at all gap distances. The levitation force increased by about five times with a gap distance of 150 and

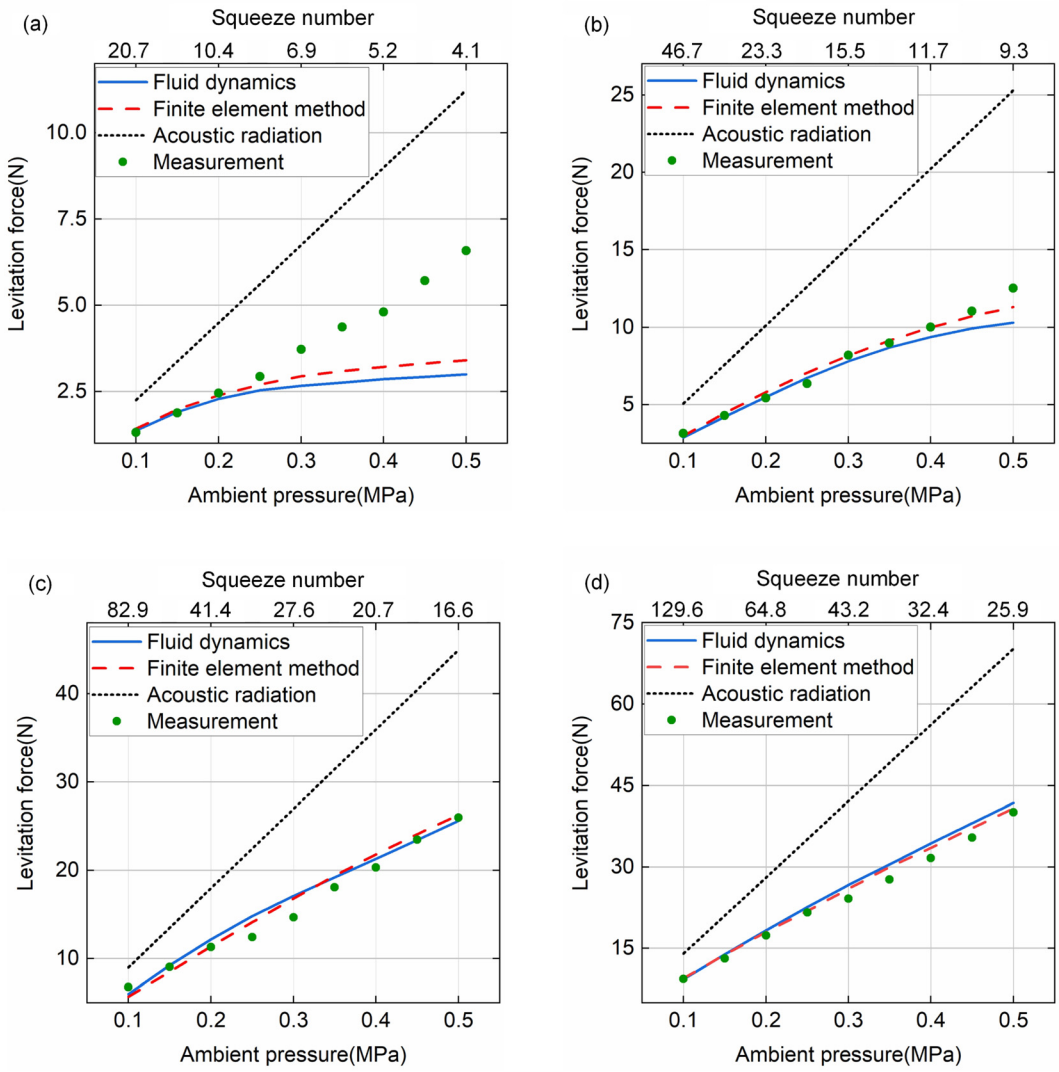

FIG. 5. Comparison of calculated and measured levitation forces at the vibration amplitude of 30 μm. (a) $h = 150$ μm. (b) $h = 100$ μm. (c) $h = 75$ μm. (d) $h = 60$ μm.

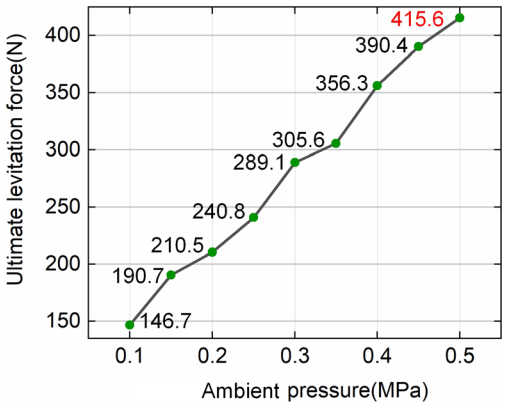

FIG. 6. The measured maximum levitation force at the minimum levitation distance.

100 μm [Figs. 5(a) and 5(b)], and about four times with a gap distance of 75 and 60 μm [Figs. 5(c) and 5(d)].

It can be observed that the one-dimensional acoustic radiation pressure model has poor agreement with measured results because the gap distance is much smaller than the sound wavelength, and the squeezing effect is in dominance. The analytical model and FEM model can both predict the levitation force accurately, except when the squeeze number is below 10.

It is worth pointing out that the gas inertia is not taken into account in these models. Therefore, the actual pressure near the edge will be higher than the calculated value, resulting in overall higher levitation force. When the levitation gap is large, such as in Fig. 5(a), the squeeze number goes below 10 at higher ambient pressure. Relatively large amount of air will flow in and out of the gap at the edge. The effect of gas inertia one the levitation pressure becomes more obvious. This is the main reason for the discrepancy observed in Fig. 5(a). With the larger squeeze number in Figs. 5(c) and 5(d), the gas exchange is negligible. Therefore, the discrepancy become smaller.

Maximum load capacity at different ambient pressures is investigated by reducing the gap distance as small as possible. The levitation force measured right before the two surfaces get into contact (when loud cracking noise occurs) is considered as the maximum load capacity. The averaged minimum gap distance is estimated at around 10 μm, since the flatness of the two surfaces is in the range of 5–10 μm. A maximum levitation force of 415.6 N is measured at an ambient pressure of 0.5 MPa, as shown in Fig. 6, which is nearly three times higher compared with the levitation force at the atmospheric pressure. The equivalent load capacity is 0.309 MPa. It surpasses the load capacity of most commercial aerostatic bearings, which commonly have the load capacity in the range of 0.098–0.196 MPa.[19]

In summary, a method to improve the NFAL force is investigated theoretically and experimentally in this paper. The test results confirm that the levitation force can be effectively improved by 4–5 times at an ambient pressure of 5 atm. Reported theoretical models are still applicable to predict the levitation force at higher ambient pressure. In principle, the NFAL bearings have most of the advantages offered by aerostatic bearings. The findings of this study could be used for applications of NFAL in contactless support and handling when the higher load capacity is required.

This research was supported by the Ningbo Science and Technology Innovation 2025 Major Special Project No. 2018B10059, Ningbo 3315 Innovation Team—Ultrasonic Impact Treatment Technology and Equipment (No. Y80929DL04), the Zhejiang Provincial Natural Science Foundation of China under Grant No. LQ22E010011, and the Natural Science Foundation of Ningbo under Grant Nos. 202003N4356 and 2021J221.

AUTHOR DECLARATIONS

Conflict of Interest

The authors declared that they have no conflicts of interest to this work. We declare that we do not have any commercial or associative interest that represents a conflict of interest in connection with the work submitted.

DATA AVAILABILITY

The data that support the findings of this study are available from the corresponding author upon reasonable request.

REFERENCES

[1]M. Wiesendanger, U. Probst, and R. Siegwart, Ph.D. thesis (École Polytechnique Fédérale de Lausanne, 2001).
[2]O. J. E. Salbu, Trans. ASME J. Basic Eng. **86**(2), 355 (1964).
[3]Z. Su and J. Wallaschek, Arch. Appl. Mech. **81**(2), 123–139 (2011).
[4]A. Minikes, I. Bucher, and S. Haber, J. Acoust. Soc. Am. **116**(1), 217–226 (2004).
[5]H. Nomura, T. Kamakura, and K. Matsuda, J. Acoust. Soc. Am. **111**(4), 1578–1583 (2002).
[6]Y. Hashimoto, Y. Koike, and S. Ueha, J. Acoust. Soc. Am. **100**(4), 2057–2061 (1996).
[7]S. Zhao, S. Mojrzisch, and J. Wallaschek, Mech. Syst. Signal Process. **36**(1), 168–181 (2013).
[8]Y. Liu, X. Sun, K. K. Sepahvand, and S. Marburg, Int. J. Mech. Sci. **200**, 106442 (2021).
[9]H. Li, Y. Hua, Q. Quan, D. Bai, Y. Wang, and Z. Deng, J. Intell. Mater. Syst. Struct. **29**(6), 1113–1119 (2018).
[10]K. Chen, S. Gao, Y. Pan, and G. Ping, Appl. Phys. Lett. **109**(12), 123503 (2016).
[11]M. Andrade, T. S. Ramos, J. C. Adamowski, and A. Marzo, Appl. Phys. Lett. **116**(5), 054104 (2020).
[12]M. Shi, X. Liu, K. Feng, K. Zhang, and M. Huang, Tribol. Trans. **63**(4), 704–719 (2020).
[13]Y. Wang and P. Guo, Appl. Phys. Lett. **118**(20), 204102 (2021).
[14]J. Li, W. Cao, P. Liu, and H. Ding, Appl. Phys. Lett. **96**(24), 243507 (2010).
[15]N. Brunetière and M. Wodtke, J. Sound Vib. **483**, 115496 (2020).
[16]C. P. Lee and T. G. Wang, J. Acoust. Soc. Am. **93**(3), 1637–1640 (1993).
[17]C. P. Lee and T. G. Wang, J. Acoust. Soc. Am. **94**(2), 1099–1109 (1993).
[18]B. J. Hamrock, *Fundamentals of Fluid Film Lubrication* (CRC Press, 1994).
[19]J. Su and K. N. Lie, Tribol. Int. **36**(10), 717–726 (2003).